IUBMB *Life*, 63(3): 175–182, March 2011

Research Communication

Protonation of Histidine 55 Affects the Oxygen Access to Heme in the Alpha Chain of the Hemoglobin from the Antarctic Fish *Trematomus bernacchii*

Leonardo Boechi[1*], Marcelo A. Martì[1*], Alessandro Vergara[2,3], Filomena Sica[2,3], Lelio Mazzarella[2,3], Dario A. Estrin[1] and Antonello Merlino[2,3]

[1]*Departamentos de Química Biologica y Química Inorgánica, Analítica y Química-Física (INQUIMAE-CONICET), Universidad de Buenos Aires, Ciudad de Buenos Aires, Argentina*

[2]*Istituto di Biostrutture e Bioimmagini (C.N.R.) via Mezzocannone 16, Napoli I-80134, Italy*

[3]*Dipartimento di Chimica "Paolo Corradini," Università degli Studi di Napoli "Federico II," Napoli, Italy*

Summary

The Root effect describes the drastic drop of oxygen affinity and loss of cooperativity at acidic pH expressed in the hemoglobins (Hb) of certain fish. The comparison between the deoxy structures of the Root effect Hb from the Antarctic fish *Trematomus bernacchii* (HbTb) at different pHs (pH = 6.2 and pH = 8.4) shows that the most significant differences are localized at the CDα region, where a salt bridge between Asp48 and His55 breaks during the low-to-high pH transition. In order to shed light on the relationship between pH, CDα loop structure and dynamics, and oxygen access to the active site in the alpha chain of HbTb, different computer simulation techniques were performed. Our results highlight the importance of the protonation of His55 in regulating oxygen access, underscoring its pivotal role in the structural and functional properties of HbTb. These data provide further support to the hypothesis that this residue might contribute to the release of Root protons in HbTb and underline the fact that an efficient transport of molecular oxygen in Hbs relies on a subtle balance of tertiary structure and protein conformational flexibility. © 2011 IUBMB IUBMB *Life*, 63(3): 175–182, 2011

Keywords *Trematomus bernacchii;* hemoglobin; implicit ligand sampling; molecular dynamics simulations; pH; oxygen binding.

Abbreviations Hb, hemoglobin; HbTb, hemoglobin from *T. bernacchii*; PDB, Protein Data Bank; PMF, potential of mean force; HbTb6, crystal structure of deoxy HbTb at pH 6.2; HbTb8, crystal structure of deoxy HbTb at pH 8.4; SB, salt bridge; VMD, visual molecular dynamics; SMD, steered molecular dynamics

INTRODUCTION

The reduced oxygen affinity of human hemoglobin (Hb) at acidic pH (the Bohr effect) represents a fundamental property of this protein that allows an efficient transport of oxygen from the lungs to the tissues. Characterization of tetrameric Hbs isolated from other species has evidenced a variety of functional modulations by pH (*1–5*). In particular, a drastic reduction oxygen-binding ability and loss of cooperativity (indicated by a Hill coefficient close to one) at acidic pH is often observed among fish Hbs (*3*). This particular behavior is called the Root effect. The occurrence of the Root effect is supposed to be linked to an overstabilization of the T-state versus the R-state at acidic pH, a fact that makes it extremely difficult to obtain structural data on the R-state at acidic pH. To investigate the structural basis for the Root effect, it is crucial to obtain structural and functional information on Hb in both R- and T-states and at different representative pH values (*6*). Consequently, the structural determinants for the Root effect and how it controls oxygen affinity remain largely unknown. Structural studies of ferrous Hbs from several temperate fish [tuna (*2*), spot (*4*) and trout (*5*)] displaying Root effect have been performed. Furthermore, several high-Antarctic fish Hbs have been characterized in both their ferrous and ferric forms, and their crystal structures have been determined (*7–17*). The Root-effect Hb isolated from the Antarctic fish *Trematomus bernacchii* (HbTb) has been used in pioneering investigations in

Additional Supporting Information may be found in the online version of this article.

*These authors contributed equally to this work.

Address correspondence to: Antonello Merlino, Dipartimento di Chimica "Paolo Corradini," Università degli Studi di Napoli "Federico II," via Cintia, I-80126 Napoli, Italy. Tel: +39081674276. Fax: +39081674090. E-mail: antonello.merlino@unina.it

Received 15 December 2010; revised 28 January 2011; accepted 28 January 2011

ISSN 1521-6543 print/ISSN 1521-6551 online
DOI: 10.1002/iub.436

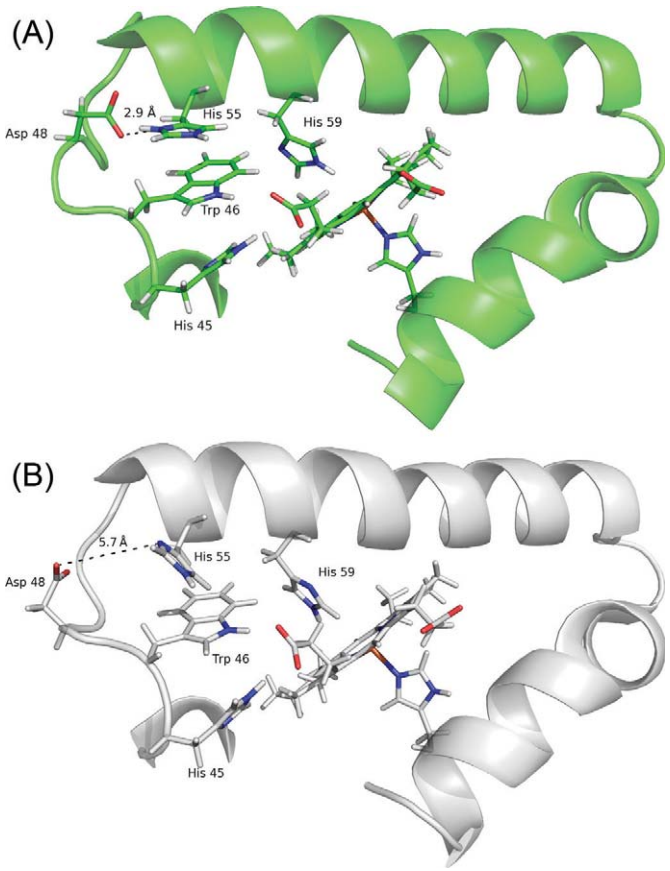

Figure 1. Ribbon representation of the CDα region in the X-ray structure of HbTb at pH = 6.2 (A) and 8.4 (B). The distance between His55 and Asp48, salt bridge, is depicted in both structures as dashed lines. [Color figure can be viewed in the online issue, which is available at wileyonlinelibrary.com.]

this field (*7–9*). For HbTb, we were able to determine structures of the deoxy form (T state) of the protein at pH = 6.2 (HbTb6) and pH = 8.4 (HbTb8) (*9*). Detailed structural analyses on these crystals revealed that the most significant differences are located in the α chains at the CDα corner, where a salt bridge (SB) between Asp48 and His55 is broken along the low-to-high pH transition, as shown in Fig. 1.

As this region is close to heme pocket, it was suggested to be involved in the R/T transition (*18, 19*), and it was proposed to play an important role in the regulation of oxygen affinity (*9, 18–20*). Although the main pathway for ligand migration in Hbs is still under discussion (*21–24*), with several groups proposing that ligands may escape through the interior of globins by multiple pathways (*22–24*), there are many experiments showing that the distal His (E7), "the so-called His gate," is the most important path for ligand entry and escape between the solvent and the heme active site (*21, 24*). Regulation of HisE7 gate movement is, therefore, a key issue for determining oxygen association rate and, therefore, affinity.

In the general context, understanding the relationship between quaternary R/T transitions in Hbs and the tertiary structural changes that alter the oxygen affinity is a formidable task, and even for the vastly studied human Hb, the connection is not completely clear. It is even less clear how and whether tertiary structure variations that occur due to changes in the environment pH (Bohr and Root effects) alter each subunit oxygen-binding properties.

During the last decade, our group performed several computational studies, using molecular dynamics (MD), including constant pH MDs, multiple steered MD and also *ab initio* electronic structure and hybrid quantum mechanics molecular mechanics (QM/MM) calculations for different members of the globin superfamily, with the aim of studying how tertiary structure and dynamics control ligand affinity. In particular, we studied how oxygen dissociation is determined by the oxygen interactions with the distal cavity, which can be dynamically regulated (*25–29*).

To advance in our understanding of the relation between tertiary structural modifications produced by a change in the pH and the oxygen affinity regulation mechanisms, we have performed a MD study of the pH-dependent structural changes in the α-chain of HbTb and their relation to oxygen access to the heme. Our results reveal interplay between the environment pH, the CD-corner conformation and the O_2 access to the active site, also suggesting an involvement of His55 protonation in the observed Root effect of this Hb.

COMPUTATIONAL METHODS

Set-up of the System

Starting structures for all MD simulations were built from crystallographic HbTb6 and HbTb8 α-chain structures (pdb codes 2H8F and 2H8D, respectively) (*9*). Four different systems were built to perform MD simulations corresponding to (*a*) HbTb α-chain with protonated His55 (HIP), using HbTb6 crystal as starting point (called αHIP); (*b*) HbTb α-chain, with deprotonated δ tautomer His55 (HID), using HbTb8 crystal as starting point (called αHID); (*c*) HbTb α-chain, with HIP, using HbTb8 crystal as starting point (we called αH2L as an acronym for High pH structure simulated a Low pH); (*d*) HbTb α-chain, with deprotonated δ tautomer His55, using HbTb6 crystal as starting point (we called αL2H). The αHIP and αHID were also used for constant pH MD simulations (CPHMD) as will be explained below. All systems were immersed in an octahedral box of waters, and the heme was simulated in the deoxy (or ligand-free) state consistent with the crystal structures.

MD Simulation Parameters

All MD simulations were carried out using the AMBER9 suite of programs (*30*). The AMBER parm99 force field (*31*) was used for all residue parameters, TIP3P was the water model, and the generalized Born implicit solvation model was used for the CPHMD. The heme deoxy parameters were the

same as those used in other works (*25–29*). Temperature was weakly coupled to a Berendsen temperature bath at 300 K with a time constant of 2 ps. Bond lengths including hydrogen were constrained by using the SHAKE algorithm allowing the use of a 2fs time step. Explicit water MD simulations were performed using Periodic Boundary conditions and Ewald sums for treating long-range electrostatic interactions while a direct cutoff for of 12 Å was applied to all nonbonded interactions. All these are commonly used parameters for this type of simulations using AMBER (*30*).

The CPHMD approach was applied as implemented in AMBER (*32*). The method addresses the dynamic dependence of pKa through Monte Carlo sampling of the Boltzmann distribution of protonation states concurrent with the MD simulations. The nature of the distribution is affected by solvent reference pH, which is set as an external parameter. In particular, at each scheduled Monte Carlo step (100 ps in our simulations), a titratable site and a new protonation state for that site are randomly chosen. The total transition energy ΔG, which depends on the local structure and reference pH, is calculated and used as the Metropolis criterion to decide if the simulation continues with previous or new protonation state. After simulation is finished, populations of each protonation state can be recovered and, therefore, the corresponding residue pKa can be computed. Aspartates, glutamates, and His55 have been titrated for the CPHMD simulations at pH = 6.2 and pH = 7, while lysines, tyrosines, and His55 for the CPHMD simulations at pH = 8.4. The CPHMD simulations were also repeated using a harmonic restraint of 1 kcal/mol/Å on Cα atoms of the protein residues to avoid partial protein denaturation due to use of implicit solvation method. This methodology was successfully applied to compute protein residues pKa values (*29*).

Equilibration and Production Simulation Protocol

For all systems, structures were first energy-minimized using steepest descent algorithm followed by the conjugate gradient algorithm giving 12,000 steps. Harmonic restraints applied to the Cα atoms were slowly relaxed from 25 to 1 kcal/mol/Å by the end of the energy minimization step. The equilibration period in the MD simulations consisted of three stages. In the first one, the system was gradually heated to 300 K for 30 ps at 100-K intervals followed by 70 ps at 300 K. The remaining restraints were gradually reduced to zero in this stage. The second stage consisted of 50 ps of unrestrained equilibration. Finally, in the third stage, 20-ns long explicit water production MD simulations were performed for the αHIP, αHID, αL2H, and αH2L systems. The CPHMD simulations were performed starting from the optimized structures but removing the explicit waters. In total, eight CPHMD simulations were performed starting from either the αHIP or αHID structures, at reference solution pH values of 6.2, 7.0, and 8.4. A summary of the simulated systems is reported in Supporting Information Table S1.

Implicit Ligand Sampling Analysis

To analyze possible oxygen entry paths from the solvent to the heme active site in αHIP and αHID, we performed implicit ligand sampling (ILS) analysis (*33*) by using the visual molecular dynamics (VMD) software package (*34*). In the ILS method, the free energy of placing an oxygen ligand in each place around and inside the protein is computed using a statistical thermodynamic approach and dividing the space in a finite grid. The results consist of free energy isosurfaces that map possible pathways for oxygen (or other ligand) migration from the solvent into the protein. The method treats the ligand as a perturbation to the protein once the protein dynamics has been already sampled (*i.e.,* the assumption is made that the ligand does not affect protein dynamics). However, it has been shown to yield quantitative results for ligand migration process when compared with more costly free energy methods that treat the ligand explicitly (*33, 35*).

Calculation of Oxygen Molecule Entry Free Energy Profile

Free energy profile of oxygen molecule access to the heme was determined in the two different structures obtained by αHIP or αHID simulations. The profiles were computed by means of constant velocity multiple steered molecular dynamics simulations, and using the Jarzinski's equality, as already done in many other works from our group [see, *e.g.*, 25, 28].

Briefly, calculations were performed using a force constant of 200 kcal/(mol $Å^2$) and a pulling velocity of 12 Å/ns. To construct the free energy profile of O_2 access to heme, a set of 20 independent steered molecular dynamics (SMD) simulations were performed. Convergence of each profile was determined by computing different exponential averages, each using an increasing number of individual work profiles, until no significant changes in the resulting free energy profile were obtained with the incorporation of new work profiles (Supporting Information Fig. S1). On the other hand, distribution of single SMD is given as another way to show convergence in the free energy profiles (Supporting Information Fig. S2). The relatively small number of SMD required to achieve convergence in the computed free energy profiles possibly reflects the fact that the ligand migration process does not imply significant protein reorganization.

RESULTS AND DISCUSSION

Protonation State of His55 Determines CDα Loop Structure and Dynamics

We begin our analysis investigating the structure and dynamics of αHIP and αHID systems, that is, the HbTb α-chain with protonated and deprotonated His55, respectively. Both simulations are stable, as shown by the root mean square deviation (RMSD) versus time plot using the starting X-ray structure as a reference (Supporting Information Fig. S3). Consistently with

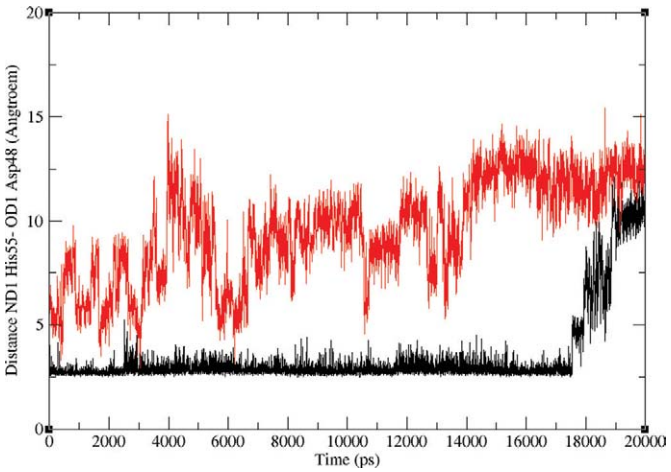

Figure 2. Time evolution of distance between the ND1 atom of His55 and the OD1 atom of Asp48, for αHIP (black, lower curve) and αHID (red, upper curve) simulations, respectively. [Color figure can be viewed in the online issue, which is available at wileyonlinelibrary.com.]

the starting crystal structures, the differences between the average conformations obtained for αHIP and αHID simulations are mainly located at the CD loop. To give a better characterization of the observed differences, the average structures obtained from the simulations (Ave_αHIP and Ave_αHID) were compared with original HbTb6 and HbTb8 crystal structures but computing the RMSD values of only the CD-loop regions (residues 48 to 55). A summary of the results for this comparison is reported in Supporting Information Table S2.

The data reveal that the differences in the CDα loop structure are conserved during the simulations. Indeed the RMSD between the CD regions in HbTb6 and Ave_αHIP and between HbTb8 and Ave_αHID are smaller (ca. 0.4 Å) than those calculated comparing the same regions of HbTb8 and Ave_αHIP and HbTb6 and Ave_αHID (0.6 to 0.8 Å). The main reason of these differences is linked to the presence/absence of the SB between Asp48 and His55 side chains (See Fig. 1). In fact, in the αHIP state, the aforementioned SB is conserved during almost the whole simulation (it is lost only in the last 2 ns, Fig. 2). On the other hand, for the αHID case, both Asp48 and His55 side chains are exposed to the solvent and the SB between these residues is not formed during the whole simulation timescale (Fig. 2). On the basis of these results, we can hypothesize that the presence of the Asp48-His55 SB is sufficient to preserve the different structure of the CDα loop observed in the crystals.

We evaluated the Cα root mean square fluctuations of both αHIP and αHID systems, to study the dynamic behavior of each residue of the protein (Supporting Information Fig. S4). As expected, most secondary structure regions show low mobility during the simulations, whereas pronounced fluctuations are observed in the loop regions. Interestingly, although αHIP and αHID present a similar fluctuation pattern, many residues, including those constituting the CD region (residues 48–55), are slightly more flexible in αHID.

To verify the relationship between the His55 protonation state, the presence of the Asp48-His55 SB and the CD loop structure, we performed two additional simulations called low-to-high (L2H) and high-to-low (H2L). The H2L simulation uses HbTb8 crystal structure as starting point (where the Asp-His interaction was not present), and His55 is in the protonated state. The H2L simulation starts from HbTb6 crystal structure (where the Asp-His interaction was present), and His55 is simulated in the deprotonated delta state.

Visual inspection of L2H simulation shows that immediately after short equilibration (less than 1 ns), the Asp48-His55 bond breaks, and Asp48 moves away from His55 toward the solvent (see Supporting Information Fig. S5), evidencing that His55 protonation is involved in the SB formation between Asp48 and His55. On the other hand, the H2L simulations reveals that protonation of His55 is not sufficient to establish the SB with Asp48, although the HIP is located closer to Asp48 (Supporting Information Fig. S5). Probably, longer simulations should be performed to obtain the correct interaction pattern. In summary, the results show that different protonation state of His55 accounts for the structural differences in the CD loop.

The His55 pKa

In the preceding simulations, the His55 protonation was fixed as protonated (HIP) or deprotonated state (HID). Although our results show that different protonation state of His55 is sufficient to account for the observed pH-dependent structural differences, a key question is whether His55 pKa has the adequate value to account for the observed transition between pH values of 6.2 and 8.0. To determine His55 pKa, we performed CPHMD simulations, starting from both HbTb6 and HbTb8 structures, and with external reference pH values of 6.2, 7.0, and 8.4. Consistent with the hypothesis that His55 should be deprotonated at pH = 8.4 and protonated at pH = 6.2, we obtained a calculated pKa value for His55 of around 6.6 (Supporting Information Table S3).

The analyses of the distance between the Oδ1 atom of Asp48 and the Nδ2 atom of His55 as function of time in the CPHMD simulations further support the conclusion that the charge of His55 is determinant for the formation of the Asp48-His55 SB, since the protonation/deprotonation of the His during the simulations is associated with frequent formation/loss of the corresponding SB (see, *e.g.*, Supporting Information Fig. S6).

CD loop-HisE7 Gate Connection

So far, we have shown that His55 protonation state controls CD structure and dynamics. Given the predicted His55 pKa of about 6.6, this residue emerges as possible main source of the Root protons. To analyze how the protonation of His55 could modulate oxygen affinity, and, that is, how the protonation state of His55 could be related to the Root effect, we analyzed

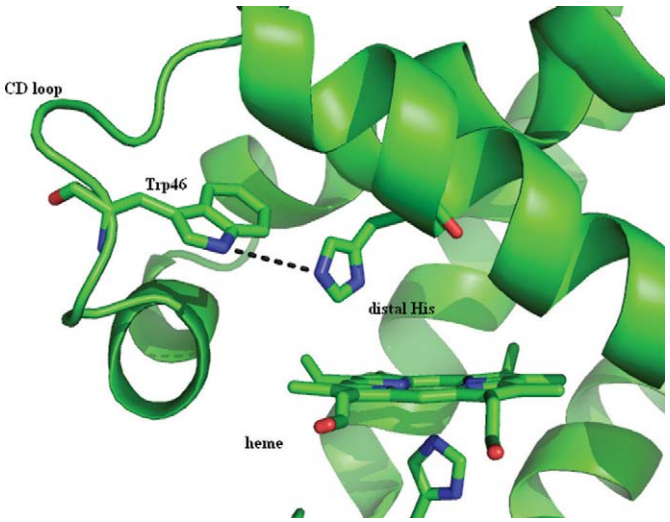

Figure 3. Open conformation of distal His in αHID representative structure. The hydrogen bond with Trp46 is shown as dashed lines. [Color figure can be viewed in the online issue, which is available at wileyonlinelibrary.com.]

whether there is a connection between the conformation of the CD region and that of residues constituting the heme pocket in αHIP and αHID. Visual inspection of the dynamics shows that there is interplay between the protonation state of His55 and the conformation of His59, which corresponds to distal HisE7 "gate" (Supporting Information Fig. S7 and Fig. 3). In this respect, it is interesting to note that a correlation between CD loop and the distal His has been also suggested for the deoxy state of myoglobin (*36*), and that CD loop displacement is proposed to be the first step along the allosteric pathway from the R to the T state in human Hb (*37*).

Our results show that when His55 is in the deprotonated state (high pH) and the SB between Asp48-His55 is broken, the CD loop is flexible and the side chain of HisE7 rotates and moves toward the solvent acquiring the so-called "open" conformation (Supporting Information Fig. S7). The swinging out of HisE7 resembles the characteristic movement predicted by Perutz for the heme pocket in human Hb (*38*), which was also observed in the X-ray structures of other globins (*39–41*), like Myoglobin (*42, 43*). A detailed inspection of the trajectories suggests that the opening of His59 (HisE7 gate) in the αHID simulation is favored by the formation of a stable hydrogen bond between NE2 of His59 and NE1 of Trp46 (Fig. 3 and Supporting Information Fig. S8) and by hydrophobic interactions that His59 itself establishes with Trp46 and Phe43. On the other hand, when His55 is protonated, a stable cluster is formed by the side chains of Trp46, Asp48, and His55. The presence of this cluster, which is observed also in the crystal structure at pH = 6.2 (Fig. 1A), reduces the

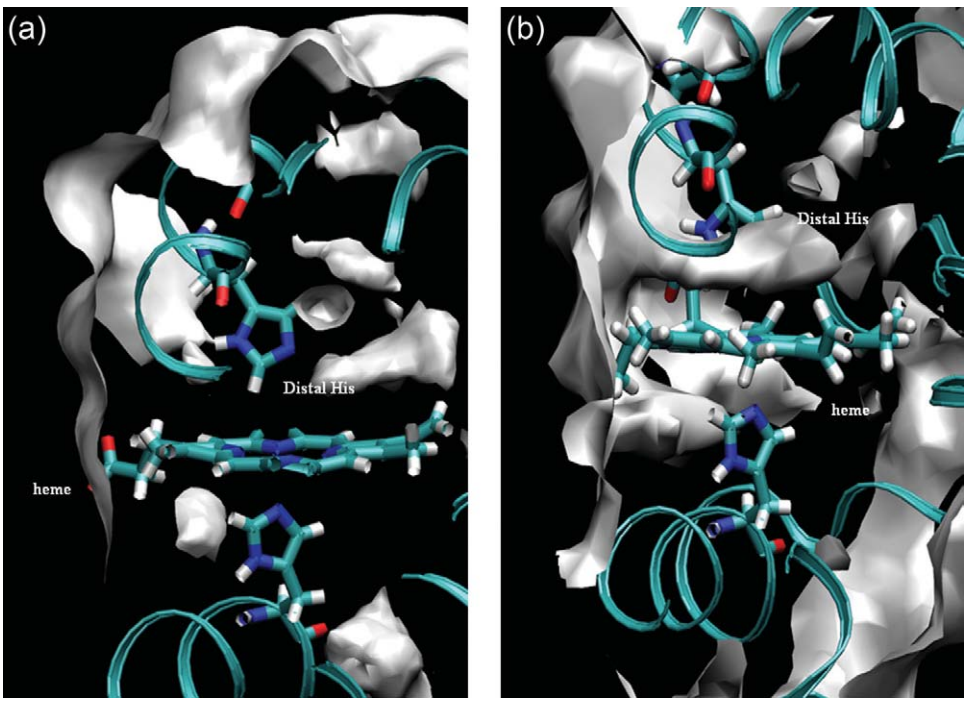

Figure 4. Implicit ligand sampling computed free energy maps for molecular oxygen migration inside the α-chain of HbTb obtained for the αHIP (A) and αHID (B) simulations, respectively. The shown isosurface represents a free energy value of −2.4 kcal/mol. The heme is displayed with the proximal and distal histidine in sticks. [Color figure can be viewed in the online issue, which is available at wileyonlinelibrary.com.]

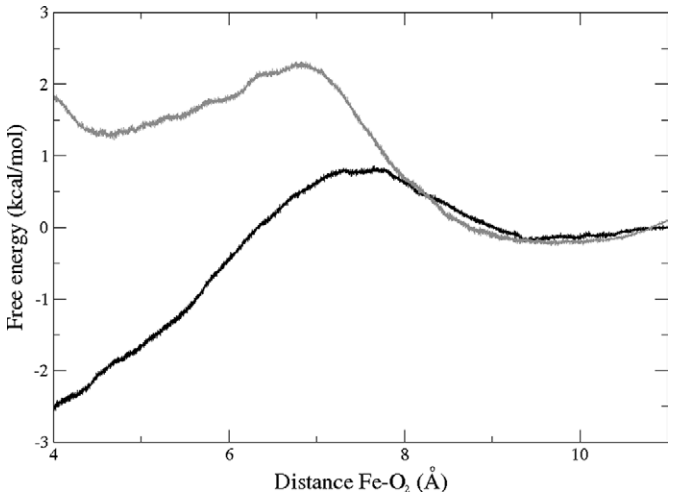

Figure 5. Free energy profiles for oxygen migration from solvent to the active site through HisE7 gate in the α-chain of HbTb at pH = 6.2 (grey) and pH = 8.4 (black).

flexibility of the CD loop and limits the conformational variations of Trp46 side chain that it not available to interact with His59. This should favor the HisE7 closed conformation at low pH.

One of the most striking consequences of these observations lies on the fact that usually HisE7 gate opening is associated with the protonation/deprotonation of the HisE7 itself, as observed for the low-pH crystal structures of Myoglobin (*42, 43*). To the best of our knowledge, this study represents the first direct evidence of the interplay between the conformation of the CD loop and that of the distal HisE7 in Root-effect Hbs. Notably, the acquisition of the distal histidine open conformation in the α-chain of HbTb should be favored at basic pH.

ILS Study of Oxygen Access to the Heme

Until this point, our results revealed a connection between the His55 protonation, and the conformation of the CD loop that is further linked to the distal HisE7 gate conformation. We now analyze whether the HisE7 open conformation observed in the αHID simulations displays a more open access to the heme iron when compared with the αHIP simulations. To analyze the presence of ligand migration paths, we computed the free energy for placing an oxygen molecule in each space region around and inside the protein with the ILS method (See Methods) using the explicit water MD simulations corresponding to the αHID and αHIP systems. The results are shown as free energy isosurfaces in Fig. 4. The results clearly show the presence of a large tunnel connecting the heme iron with the solvent in the αHID system. The specific pathway starts in a cavity close to His55, Phe43, Ala58, and Lys62 and reaches the heme. On the other hand, no continuous path connecting the solvent with the heme iron is observed for the αHIP system, even at high free energy values. This is in line with the fact that we did not observe any opening of the distal His during the αHIP simulation.

Free Energy Profile for O_2 Access to the Heme

To obtain a quantitative measure of the oxygen ligand entry process, we computed free energy profiles for O_2 access to the distal cavity from the solvent, in both pH states corresponding to the HisE7 open and closed conformations. The results shown in Fig. 5 confirm the ILS suggestions. At pH = 8.4, the HisE7 adopts the open conformation and after a small (less than 1 kcal/mol) barrier, the oxygen is captured by an −2.5 kcal/mol well. On the other hand, at pH = 6.2, the HisE7 assumes the closed conformation, producing a 2.5 kcal/mol barrier, and the energy of the distal cavity is about 1.5 kcal/mol higher than the solvent. The results clearly show that the different conformations of HisE7 affect the free energy profile for O_2 access to the distal cavity from the solvent (Fig. 5). Although these results are limited to a single chain of HbTb and to ligand diffusion toward the distal cavity, they are in line with the experimental thermodynamic data, which show a reduction of oxygen affinity for HbTb at acid pH.

CONCLUSIONS

The relationship between protonation state of His55, conformation of CD corner and oxygen entry to heme pocket in the α-chain of HbTb has been studied using computer simulations. Our data provide a clear picture of the correlation between the swing motion of His59 (HisE7), the protonation/deprotonation of His55 and the structure/dynamic modifications of the CDα region, suggesting a path for oxygen diffusion to/from the heme. Although our findings are limited to the study of tertiary structure modifications within the isolated α-chain, they suggest that a fine tuning of the structure and dynamics of CDα loop provides a mechanism to modulate HbTb O_2 affinity, supporting the hypothesis that this region could play a role in the Root effect (*10, 11*). It can be envisaged that, at the high pH, when His55 is deprotonated, the CD region of the α-chain of HbTb undergoes to structural modifications that favor the open conformation of the distal His (His59), facilitating the entry of the ligand to the active site. On the contrary, when His55 is protonated, the O_2 access to heme pocket should be restricted by a slight increase in the free energy, caused by the closed conformation of distal His. In conclusion, these data suggest that His55 residue may provide Root effect protons and that its protonation/deprotonation may influence the oxygen affinity in HbTb. In a more general perspective, our results underline the fact that an efficient transport of molecular oxygen in globins relies on a subtle balance of tertiary structure and protein conformational flexibility.

ACKNOWLEDGEMENTS

This work was financially supported by PNRA (Italian National Program for Antarctic Research). It is in the framework of the program Evolution and Biodiversity in the Antarctic (EBA), sponsored by the Scientific Committee for Antarctic Research (SCAR). A.M. acknowledges the University of Naples for travel grants and University of Buenos Aires for hospitality. D.A.E. and M.A.M. are members of CONICET. L.B. holds a CONI-

CET Doctoral fellowship. Financial support was provided by Grants ANPCYT 07-1650 and UBACyT 2010-2012 to M.A.M. and Conicet PIP 01207 to D.A.E. Computer power was provided by CECAR, at FCEN UBA.

REFERENCES

1. Perutz, M. F., Fermi, G., Luisi, B., Shaanan, B., and Liddington, R. C. (1987). Stereochemistry of cooperative mechanisms in hemoglobin. *Acc. Chem. Res.* **9**, 309–321.
2. Yokoyama, T., Chong, K. T., Miyazaki, G., Morimoto, H., Shih, D. T. B., Unzai, S., Tame, J. R. H., and Park, S. Y. (2004) Novel mechanisms of pH sensitivity in Tuna hemoglobin: a structural explanation of the Root effect. *J. Biol. Chem.* **279**, 28632–28640.
3. Brittain, T. (2005) The Root effect in hemoglobins. *J. Inorg. Biochem.* **99**, 120–129.
4. Tame, J. R., Wilson, J. C., and Weber, R. E. The crystal structures of trout Hb I in the deoxy and carbonmonoxy forms. *J. Mol. Biol.* **259**, 749–760.
5. Mylvaganam, S. E., Bonaventura, C., Bonaventura, J., and Getzoff, E. D. (1996) Structural basis for the Root effect in hemoglobin. *Nature Struct. Biol.* **3**, 275–283.
6. Berenbrink, M., Koldkiaer, P., Kepp, O., and Cossins, A. R. (2005) Evolution of oxygen secretion in fishes and the emergence of a complex physiological system. *Science* **307**, 1752–1757.
7. Camardella, L., Caruso, C., D'Avino, R., di Prisco, G., Rutigliano, B., Tamburini, M., Fermi, G., and Perutz, M. F. (1992) Hemoglobin of the Antarctic fish *Pagothenia bernacchii*. Amino acid sequence, oxygen equilibria and crystal structure of its carbonmonoxy derivative. *J. Mol. Biol.* **224**, 449–460.
8. Ito, N., Komiyama, N. H., and Fermi, G. (1995) Structure of deoxyhemoglobin of the Antarctic fish *Pagothenia bernacchii* with an analysis of the structural basis of the Root effect by comparison of the liganded and unliganded hemoglobin structures. *J. Mol. Biol.* **250**, 648–658.
9. Mazzarella, L., Vergara, A., Vitagliano, L., Merlino, A., Bonomi, G., Scala, S., Verde, C., and di Prisco, G. (2006) High resolution crystal structure of deoxy haemoglobin from *Trematomus bernacchii* at different pH values: the role of histidine residues in modulating the strength of the Root effect. *Proteins: Struct. Funct. Bioinf.* **65**, 490–498.
10. Mazzarella, L., Bonomi, G., Lubrano, M. C., Merlino, A., Riccio, A., Vergara, A., Vitagliano, L., Verde, C., and di Prisco, G. (2006) Minimal structural requirements for root effect: crystal structure of the cathodic hemoglobin isolated from the antarctic fish *Trematomus newnesi*. *Proteins: Struct. Funct. Bioinf.* **62**, 316–321.
11. Vergara, A., Vitagliano, L., Merlino, A., Sica, F., Marino, K., Verde, C., di Prisco, G., and Mazzarella, L. (2010) An order-disorder transition plays a role in switching off the Root effect in fish hemoglobins. *J. Biol. Chem.* **285**, 32568–32575.
12. Mazzarella, L., D'Avino, R., di Prisco, G., Savino, C., Vitagliano, L., Moody, P. C., and Zagari, A. (1999) Crystal structure of *Trematomus newnesi* haemoglobin re-opens the Root effect question. *J. Mol. Biol.* **287**, 897–906.
13. Merlino, A., Verde, C., di Prisco, G., Mazzarella, L., and Vergara, A. (2008) Reduction of ferric hemoglobin from *Trematomus bernacchii* in a partial bis-histidyl state produces a deoxy coordination even when encapsulated into the crystal phase. *Spectroscopy* **22**, 143–152.
14. Merlino, A., Vitagliano, L., Howes, B., Verde, C., di Prisco, G., Smulevich, G., Sica, F., and Vergara, A. (2009) Combined crystallographic and spectroscopic analysis of *Trematomus bernacchii* hemoglobin highlights analogies and differences in the peculiar oxidation pathway of Antarctic fish hemoglobins. *Biopolymers* **91**, 1117–1125.
15. Vergara, A., Franzese, M., Merlino, A., Bonomi, G., Verde, C., Giordano, D., di Prisco, G., Lee, H. C., Peisach, J., and Mazzarella, L. (2009) Correlation between hemichrome stability and the Root effect in tetrameric hemoglobins. *Biophys. J.* **97**, 866–874.
16. Vergara, A., Franzese, M., Merlino, A., Vitagliano, L., Verde, C., di Prisco, G., Lee, H. C., Peisach, J., and Mazzarella, L. (2007) Structural characterization of ferric hemoglobins from three Antarctic fish species of the suborder Notothenioidei. *Biophys. J.* **93**, 2822–2829.
17. Vitagliano, L., Vergara, A., Bonomi, G., Merlino, A., Verde, C., di Prisco, G., Howes, B. D., Smulevich, G., and Mazzarella, L. (2008) Spectroscopic and crystallographic characterization of a tetrameric hemoglobin oxidation reveals structural features of the functional intermediate relaxed/tense state. *J. Am. Chem. Soc.* **130**, 10527–10535.
18. Baldwin, J. and Chothia, C. (1979) Hemoglobin: the structural changes related to ligand binding and its allosteric mechanism. *J. Mol. Biol.* **129**, 175–220.
19. Ackers, G. K. (1998) Deciphering the molecular code of hemoglobin allostery. *Adv. Prot. Chem.* **51**, 185–253.
20. Merlino, A., Vergara, A., Sica, F., Aschi, M., Amadei, A., Di Nola, A., and Mazzarella, L. (2010) Free-energy profile for CO binding to separated chains of human and *Trematomus newnesi* hemoglobin: insights from molecular dynamics simulations and perturbed matrix method. *J. Phys. Chem. B* **114**, 7002–7008.
21. Scott, E. E., Gibson, Q. H., and Olson, J. S. (2010) Distal histidine stabilizes bound O_2 and acts as a gate for ligand entry in both subunits of adult human hemoglobin. *J. Biol. Chem.* **285**, 8840–8854.
22. Tilton, R. F., Jr., Kuntz, I. D., Jr., and Petsko, G. A. (1984). Cavities in proteins: structure of a metmyoglobin-xenon complex solved to 1.9 Å. *Biochemistry* **23**, 2849–2857.
23. Tilton, R. F., Jr., Singh, U. C., Kuntz, I. D., Jr., and Kollman, P. A. (1988). Protein-ligand dynamics. A 96 picosecond simulation of a myoglobin-xenon complex. *J. Mol. Biol.* **199**, 195–211.
24. Elber, R. and Karplus, M. (1990) Enhanced sampling in molecular dynamics: use of the time-dependent Hartree approximation for a simulation of carbon monoxide diffusion through myoglobin. *J. Am. Chem. Soc.* **112**, 9161–9175.
25. Boechi, L., Martí, M. A., Milani, M., Bolognesi, M., Luque, F. J., and Estrin, D. A. (2008) Structural determinants of ligand migration in *Mycobacterium tuberculosis* truncated hemoglobin O. *Proteins Struct. Funct. Bioinf.* **73**, 372–379.
26. Capece, L., Estrin, D. A., and Marti, M. A. (2008) Dynamical characterization of the heme NO oxygen binding (HNOX) domain. Insight into soluble guanylate cyclase allosteric transition. *Biochemistry* **47**, 9416–9427.
27. Perissinotti, L. L., Marti, M. A., Doctorovich, F., Luque, F. J., and Estrin, D. A. (2008) A microscopic study of the deoxyhemoglobin-catalyzed generation of nitric oxide from nitrite anion. *Biochemistry* **47**, 9793–9802.
28. Capece, L., Marti, M. A., Bidon-Chanal, A., Nadra, A., Luque, F. J., and Estrin, D. A. (2009) High pressure reveals structural determinants for globin hexacoordination: neuroglobin and myoglobin cases. *Proteins Struct. Funct. Bioinf.* **75**, 885–894.
29. Martí, M. A., Estrin, D. A., and Roitberg, A. E. (2009) Molecular basis for the pH dependent structural transition of Nitrophorin 4. *J. Phys. Chem. B* **113**, 2135–2142.
30. Pearlman, D. A., Case, D. A., Caldwell, J. W., Ross, W. S., Cheatham Iii, T. E., DeBolt, S.; Ferguson, D., Seibel, G., and Kollman, P. (1995) Amber, a Package of *Computer*-Programs for Applying Molecular Mechanics, normal mode analysis, molecular dynamics and free energy calculations to simulate the structural and energetic properties of molecules. *Comp. Phys. Comm.* **91**, 1–3, 1–41.
31. Hornak, V., Abel, R., Okur, A., Strockbine, B., Roitberg, A., and Simmerling, C. (2006) Comparison of multiple Amber force field and development of improved protein backbone parameters. *Proteins: Struct. Funct. Genet.* **65**, 712–725.

32. Mongan, J., Case, D. A., McCammon, J. A. (2004) Constant pH molecular dynamics in generalized born implicit solvent. *J. Comput. Chem.* **25**, 2038–2048.
33. Cohen, J., Olsen, K. W., and Schulten, K. (2008) Finding gas migration pathways in proteins using implicit ligand sampling. *Methods Enzymol.* **437**, 439–457.
34. Humphrey, W., Dalke, A., and Schulten, K. (1996) VMD-visual molecular dynamics. *J. Mol. Graph.* **14**, 33–38.
35. Lama, A., Pawaria, S., Bidon-Chanal, A., Anand, A., Gelpí, J. L., Arya, S., Martí, M., Estrin, D. A., Luque, F. J., and Dikshit, K. L. (2009) Role of Pre-A motif in nitric oxide scavenging by truncated hemoglobin, HbN, of *Mycobacterium tuberculosis*. *J. Biol. Chem.* **284**, 14457–14468.
36. Guallar, V., Jarzecki, A. A., Friesner, R. A., and Spiro, T. G. (2006) Modeling of ligation-induced helix/loop displacements in myoglobin: toward an understanding of hemoglobin allostery. *J. Am. Chem. Soc.* **128**, 5427–5435.
37. Alcantara, R. E., Xu, C., Spiro, T. G., and Guallar, V. (2007) A quantum-chemical picture of hemoglobin affinity. *Proc. Natl. Acad. Sci. USA* **104**, 18451–18455.
38. Perutz, M. F. (1989) Mechanisms of cooperativity and allosteric regulation in proteins. *Q. Rev. Biophys.* **22**, 139–237.
39. Vallone, B., Nienhaus, K., Mattheus, A., Brunori, M., and Nienhaus, G. U. (2004) The structure of carbonmonoxy neuroglobin reveals a heme-sliding mechanism for control of ligand affinity. *Proc. Natl. Acad. Sci. USA.* **101**, 17351–17356.
40. Jenkins, J. D., Mausayev, F. N., Danso-Danquah, R., Abraham, D. J., and Safo, M. K. (2009) Structure of relaxed-state of human haemoglobin:insight into ligand uptake, transport and release. *Acta Cryst. D* **65**, 41–48.
41. Olson, J. S., Soman, J., and Philips, G. N. (2007) Ligand pathways in Myoglobin: a review of Trp cavity mutations. *IUBMB Life* **59**, 552–562.
42. Yang, F. and Phillips, G. N., Jr. (1996) Crystal structures of CO-, deoxy- and met-myoglobins at various pH values. *J. Mol. Biol.* **256**, 762–774.
43. Scott, E. E., Gibson, Q. H., and Olson, J. S. (2001). Mapping the pathway for O_2 entry into and exit from myoglobin. *J. Biol. Chem.* **276**, 5177–5188.